

Contents lists available at Dergipark

Journal of Scientific Reports-A

journal homepage: https://dergipark.org.tr/tr/pub/jsr-a



E-ISSN: 2687-6167 Number 62, September 2025

RESEARCH ARTICLE

Tuning the magnetization by preserving half-metallicity of FeCl₂ via embedding transition metal atoms: a DFT study

Ali Emre GENÇa*

^aGazi University, Department of Physics, 06500, Teknikokullar/Ankara, ORCID: 0000-0001-9567-2018

Abstract

In this article, the varying magnetization of the modified FeCl₂ two-dimensional (2D) layers have been investigated through Density Functional Theory calculations with and without DFT+U method.. Following the optimizations and post-processing electronic analyses regarding the FeCl₂ bulk, the two-dimensional layer was created, and the 3d group of transition metal (TM) atoms (from Sc to Ni) were embedded into the defective Cl position in line with the experimental works. The calculations show that while each Fe atom in FeCl₂ has $4.00 \mu_B$ magnetization in the pure layer, after embedding transition metal atoms, this value varies in a broad range between 8 to 19 μ_B in completely FM (ferromagnetic) ground state based on only DFT calculations. Between these TMembedded layers, Ti embedded FeCl2 layer showed half-metallicity in one of two spin channels with and without DFT+U calculations, a prerequisite for spintronic applications. The Projected Density of States (PDOS) of Ti embedded layer, t2g orbitals (d_{xy}, d_{xz}, and d_{yz}) of the neighboring Fe atoms are responsible for the conductivity in the spin-down channel based on DFT calculations. The hubbard parameters completely changes the picture where the non-neighboring atom contribution to the conductive electronic states are dominant. These findings are supported by band gap curves. The bond type identification has been elucidated by ICOHP (integrated crystal orbital Hamiltonian population) and ICOBI (integrated crystal orbital bond index) parameters. PDOS (partial density of states) and pCOHP (partial crystal orbital Hamiltonian) plots were used to identify which bonding-antibonding orbitals were populated. Finally, embedding Ti into Cl defect positions can induce different magnetization levels by preserving half metallicity while the other layers do not provide half-metallicity. © 2023 DPU All rights reserved.

Keywords: Density functional theory; spintronics; 2D materials; transition metal embedding; FeCl₂; transition metal dihalides.

^{*} Corresponding author. Tel.: +0-000-000-0000 ; fax: +0-000-000-0000 . *E-mail address: aegenc@gazi.edu.tr*

1. Introduction

Materials with valuable properties for spintronic applications have been explored due to offering offer advantages over conventional electronics regarding data transfer and storage [1]. Prerequisites of smaller-than-expected gadgets roused the specialists to plan two-layered materials offering multifunctional qualities, particularly by preserving the data in the type of twist quantum values instead of electrical charge [2]. In this context, spintronic appeared as a new field where half-metallicity plays a vital role presenting plenty of prospects that may be utilized in diverse applications like fast data storage and data processing, etc[3]. Since the invention of Graphene, which led the way for the creation of other similar materials, many 2-D counterparts have been investigated for their spintronic applications, such as g- G_3N_4 nanosheets, BN and AlN monolayers, and N-doped graphene [4-7]. Apart from these single-layer 2-D materials, magnetic Van der Waals materials exhibit easily exfoliated bulk structures and tunable magnetic anisotropy, making these materials promising candidates for spintronic applications [8-10].

Among these materials, TMCl₂-type (TM= transition metal) dihalides, FeCl₂ shows easiness of exfoliation experimentally and magnetization and half-metallicity 2-D [10, 11]. In one of the studies of Torun and co-workers, the 1T-FeCl₂ layer is predicted as more stable via Phonon calculations than 1H-FeCl₂ (hegzagonal) with a half-metallic behavior accompanied by 17 K Curie temperature [12]. According to the experiment in which the 2-D FeCl₂ has been synthesized, 2-D FeCl₂ moieties are observed on Au(111) single-crystal surfaces through MBE (Molecular Beam Epitaxy Method). Another exciting feature of this synthesis is that the FeCl₂ monolayer has Fe and Cl point defects that do not affect the material's structural order [11]. So far, different degrees of magnetization have been obtained over a wide range of materials [8].

In this article, FeCl₂ monolayer is used as a benchmark to reveal magnetic properties after embedding a 3d group of transition metals with DFT and DFT+U computations. As known, embedding or doping foreign atoms in the place of the surface defects is a widely used technique for magnetic adjustment [8, 13]. In the FeCl₂ 2-D monolayer, since the Cl atoms enclose Fe atoms, Cl defects are more likely to possess a more controllable structure. They are easily doped with foreign atoms without having a more complex potential energy surface. As shown in the subsequent chapters, embedding TM atoms will induce different magnetic moments by mostly destroying the half-metallicity except Ti embedded FeCl₂ layer, which is indispensable for spintronic applications. According to our results, even if some of the TM atoms induce different amounts of magnetism concerning the bare and Fe-embedded FeCl₂, half metallicity is lost. For the other layers, the electronic behavior is changed depending upon the Hubbard parameter usage mostly from metallic to semiconductive or vice versa. To our knowledge, embedding the single TM atom for adjusting the magnetic properties of the FeCl₂ monolayer has yet to be investigated in the literature. Our findings are original and might be used to create the desired spintronic devices.

2. Computational Methods

Periodic density functional theory (DFT) calculations were examined through the Quantum Espresso simulation package [14-16]. Electron-ion interactions were softened via PAW-type pseudopotentials, while the exchange-correlation effect was treated by PBE functional [17-19]. The values of 80 Ry for cut-off and 800 Ry for kinetic energy cut-off have been considered adequate for extending plane waves over the Brillouin zone. The Gaussian smearing for Brillouin Zone integration has been used as 0.01 Ry degauss value has been used. The Monkhorst-Pack k-point set has been used as 4x4x1, 6x6x1, and 8x8x1 for FeCl₂ bulk, FeCl₂ monolayer, and elaborate electronic analyses, respectively(i.e., band structure calculations, partial density of states (PDOS), and Crystal Orbital Hamilton Population (COHP) analysis) [20-23]. A vacuum length has been taken as 32 Å to complete the elimination of the unwanted interactions along the z-direction. Grimme-D3 dispersion (Van der Waals) correction has been considered to obtain better geometries and energies, especially for FeCl₂ bulk calculations. The structural relaxations for surface-molecule interactions ceased after reaching the convergence thresholds for ionic minimizations, self-consistency, and atomic forces of 10⁻⁶Ry, 10⁻⁶Ry, and 10⁻⁶ Ry/Bohr, respectively. In all cases, different initial magnetic orders, such as FM, AFM1 and AFM2 have been taken into consideration to have better ground state descriptions, which will

be given and discussed in subsequent chapters. Following the FeCl₂ bulk calculations, one of the Cl-Fe-Cl parts of FeCl₂ has been separated for further analyses and expanded into a 2x2 supercell. Formation energies have been calculated to verify whether these TM-embedded structures can be synthesized experimentally based on Equation (1).

$$E_f = E_{system} + E_{cl} - E_{TM-atom} - E_{TM-FeCl}$$
 (1)

In Equation (1), the 1st term represents the total energy of the bare monolayer, and the 2nd, 3rd, and 4th terms are the total chemical potentials of the Cl atom, TM atoms, and the TM embedded FeCl₂. Adsorption energies were calculated according to Equation (2),

$$E_{ads} = E_{TM-FeCl_2} - (E_{FeCl_2} + E_{TM}) \tag{2}$$

In Equation (2), the 1^{st} , 2^{nd} , and 3^{rd} terms are the total energies of the interacted system, FeCl₂ monolayer, and single atom energies of the transition metals.

Charge Density Differences (CDD) were calculated by subtracting the individual charge densities of the adsorbates and of the functionalized graphene layer from the interacted system:

$$\Delta \rho_{ads} = \rho_{system} - \rho_{adsorbates} - \rho_{MnN_x O_y} \tag{3}$$

Chemical bonding information, mainly focused on elucidating the bonding nature in layers, has been acquired by applying the Crystal Orbital Hamilton Population (COHP) method. This method utilizes electronic wave functions to generate bonding information, as documented in references [24-29]. The Crystal Orbital Bond Index (ICOBI) is a novel metric that characterizes the bonds based on the Wiberg and Mayer bond index adapted for crystals [30-32]. Analyzing chemical bonding information involves considering Integrated Crystal Orbital Hamilton Population (ICOHP) and Integrated Crystal Orbital Bond Index (ICOBI) values. In the case of ICOHP, increasingly negative values indicate a higher covalent character and a stronger bond, while less negative values signify more ionic character. For ICOBI, a value close to one represents a nearly perfect covalent bond, whereas a value close to zero indicates an almost perfect ionic bond. Additionally, both ICOHP and ICOBI allow for examining orbital-projected contributions to overall quantities. Crystal Orbital Hamilton Populations (COHP) plots were employed to scrutinize electron densities over bonding and antibonding orbitals parallel to a Partial Density of States (PDOS). The calculations for COHP in this study were conducted using the Lobster code version 4.0.0[33], and the total ICOHP value for each bond was obtained by summing spin-up and spin-down components. Figures were generated using the Material Studio 6.0 interface [34].

3. Results and Discussion

The structural relaxation of the FeCl₂ bulk structure with various magnetic ordering can be seen in Fig. 1a. According to the literature, since the arrangement 1T (such as TaS_2 , VS_2 , $HfSe_2$) phase is more stable than 1H, 1 T structure has been taken as a basis can be seen in Fig. 1[12]. In this step, the same and different spin configurations for Fe and Cl atoms to break spin symmetry have been given as input in FM (Fe \uparrow , Cl \uparrow) and AFM (Fe \uparrow , Cl \downarrow) configurations.

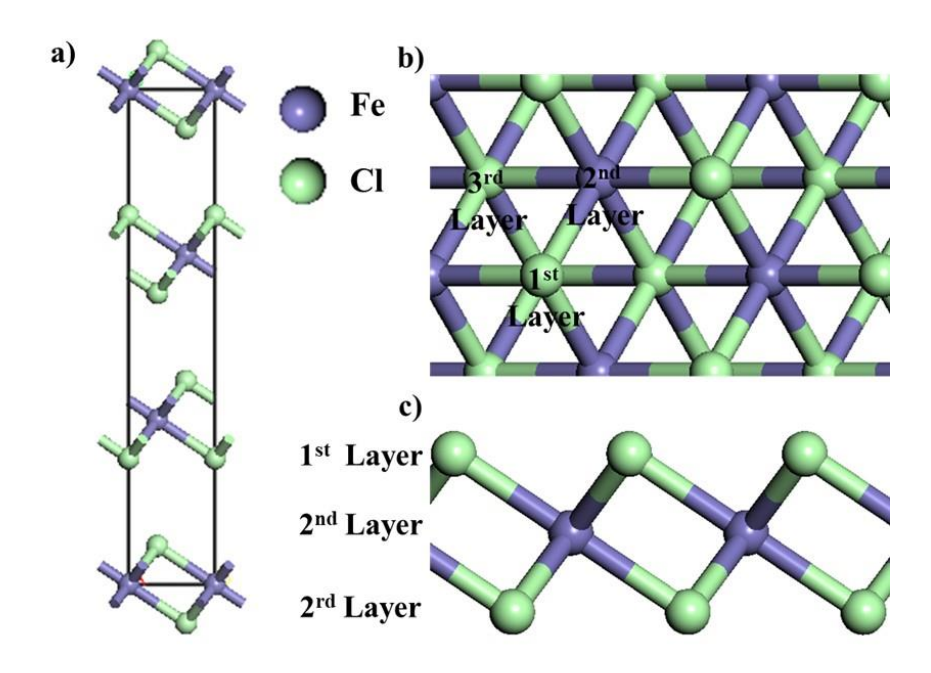


Fig. 1. (a) bulk FeCl₂ (b) top and (c) side view of the FeCl₂ crystal. Purple and light green balls represent Iron and Chlorine atoms, respectively.

Calculations based on FM and AFM spin orders gave similar energies with a difference of 10.3 meV, whereas the AFM order has lower energy, which is consistent with the literature[8]. Some structural parameters are listed in Table 1. d* is the distance between Cl atoms in the interface of the adjacent FeCl2 layer in z-direction. The atomic charges on Fe atoms are donated to Cl atoms, which make these interactions ionic.

Table 1. Calculated parameters of FeCl₂ bulk structure. ΔE_{total} is the total energy difference based on the AFM order total energy. d and d* distances show the Cl-Cl distance in a single layer and interface

FeCl ₂ -Magnetic Phases	$\begin{array}{c} \Delta E_{total} \\ \text{(meV)} \end{array}$	$ \begin{array}{c} \text{Lattice} \\ \text{Parameters} \\ \text{(a=b)} \end{array} \qquad \begin{array}{c} d_{\text{Fe}} \\ \text{cl}(\mathring{A}) \end{array} $		d _{CI} - CI(Å)	d * _{СІ-} сі(Å)		
FM	+10.3	3.54	2.47	3.43	3.73	1.10/-0.55	
AFM	0	3.54	2.47	3.43	3.73	1.10/-0.55	

In the subsequent step, a bare 2D FeCl₂ monolayer was created by isolating the layer already included in the bulk material. Because the lateral interactions might have affected the embedded single TM atom behavior in the layer, the 2x2 supercell was created in Fig. 1b and c. Before embedding TM atoms, some fundamental properties of the pure FeCl₂ layer were investigated to establish our calculations' reliability. First, the FeCl₂ layer was relaxed, and then, electronic properties were studied. Chemical bonding analyses have also been used to show the new bonding

environment of the TM with its environment. Table 2 shows some physical and chemical parameters of the isolated and pure $FeCl_2$ layer.

Table 2. Calculated parameters of free-standing FeCl₂ layer. ICOHP and ICOBI quantities are based on any Cl atom at facet and summed over its 3 Fe neighbors, d is the distance between atoms, Q is the atomic charge and μ_B is the magnetic moment

FeCl ₂ (2x2) Super Cell	Lattice Parameters (a=b)	d _{Fe-} ci(Å)	d _{Cl} . cı(Å)	Q(Fe)/Q(Cl) (e)	ICOHP (eV)	ICOBI	μ _B (cell) μ _B (f.u.)	μ _B (Fe)	μ _B (Cl)
	7.08	2.47	3.45	-1.11/0.55	-4.02	0.07	16.00 4.00	3.50	0.15

Upon relaxation of the pure FeCl₂ layer, the values related to atomic charges and distances between Fe-Cl and Cl-Cl bonds remain unchanged. When the chemical bond strengths and bond types are considered between Fe-Cl bonds, one can see that Fe-Cl bonds are mainly ionic based on 0.07 ICOBI value with a minute non-ionic contribution[30]. Moreover, the ICOHP value is -4.02 eV for the Fe and three Cl neighbors as a total, which implies that there is mostly an ionic bond type. However, this value should be compared to understand its meaningful variations depending on different TM embedding processes. Finally, the magnetic moment of the 2x2 supercell is measured to have 16.00 µB, which shows FM behavior [35]. In line with the literature, the spin-up channel has a semiconducting behavior, while the spin-down channel has a conductive based on the spin-projected Total Density of States (TDOS), which can be seen in Figure 2a. As clearly understood from Figure 2a, the bare FeCl₂ monolayer has a half-metallic behavior in which the conduction takes place on one of the spin channels. Based on the band structure plots in Fig. S1, there is no electron conductance in the spin-up channel, while spin-down electrons provide conductivity for pure FeCl₂ monolayer[12]. Band gap for pure FeCl₂ layer has been calculated to be 4.46 eV which is slightly higher than previously calculated value 4.40 eV [12]. As opposed to our finding, Yang et al found the ground state as insulator and band gap with 3.45 eV with Spin-Orbit Coupling effect [36]. From the TDOS and PDOS curves drawn by summing the contributions of all atoms in the lattice, conductive behavior at around the Fermi level is brought mainly by the Fe atoms, and there is a minute Cl contribution to half metallicity around the Fermi level. Moreover, it is pretty clear that Fe-Cl interactions are negligible and non-bonding characters at the Fermi level from Fig. 2a and 2b. Below the fermi level, a peak around 1.75 eV shows strong antibonding interactions between Fe-Cl atoms on a spin-up channel based on the -pCOHP curve in Fig. 2b. When low-lying electronic states are considered because of the different peak heights between Fe and Cl atoms, one can conclude that the interactions are mainly ionic. Around -3 eV, Cl-Fe interactions are antibonding because of the peak at ~-2.5 eV on the -pCOHP curve. In line with Table 2, spin density is mainly observed on Fe atoms on the monolayer, even if only a tiny part is accumulated on Cl atoms, as shown in Figure 2c.

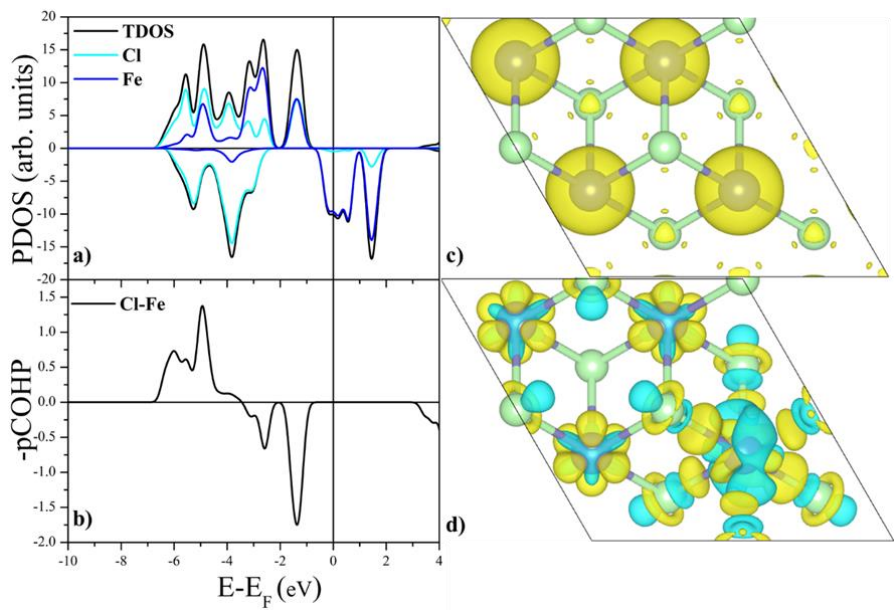


Fig. 2. (a) total density of states (TDOS) and partial density of states (PDOS) over the whole Cl (2p) and Fe (3d) atoms. (b) –pCOHP (Partial Crystal Orbital Hamilton Populations) curve belonging to the surface 1 Cl and its 3 Fe neighbors. (c) spin density and (d) charge density differences (CDD) plot of the pure FeCl₂ layer. Yellow and cyan colors represent the electron accumulation and depletion in space, respectively. Isosurface values are 0.011 *e/Bohr*⁻³ for spin density and 0.0018 *e/Bohr*⁻³ for charge density differences (CDD), respectively. In the PDOS plot, while black lines show TDOS, cyan, and blue curves correspond to the Cl and Fe atoms, respectively.

Figure 2d gives valuable information regarding electron transfer direction between atomic components. As seen, electron transfer is bidirectional since electron accumulation and depletion are observed for both atomic species. Therefore, this phenomenon is explained by the electron donation-back donation rule[37, 38]. Before embedding transition metal into the Cl defects, proven with experimental studies, it will be helpful to visualize the 2x2 supercell model and interactions in Figure 3.

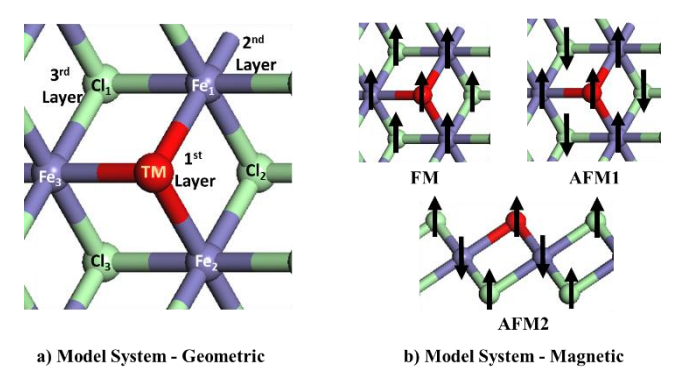


Fig. 3. (a) geometric model and (b) initial magnetic order for pure FeCl₂ and TM embedded FeCl₂ (TM-FeCl₂).

In this step, the Cl atom on the facet is replaced with whole TM atoms from Sc to Ni, respectively. In the geometric model, one of the Cl atoms on the top of the layer is substituted with TM atoms at the first layer, and its interactions with its neighbors will be explored. The magnetic model considers two different spin orders at initial configurations. For the FM order, all starting spins are given in the up direction for all atoms. In AFM1 order, all Fe atoms are shown in an up direction while spin-down directions have been considered for the Cl atoms seen in Figure 3b. In the AFM2 model, while the Cl atoms including embedded TM have up spins, the sandwiched Fe atoms have down spins in the starting configurations.

Table 3. Calculated parameters of free-standing TM embedded FeCl₂ layer. ICOHP and ICOBI quantites are averaged over the bonds with nearest neighbors.

Transition Metals	Ground Magnetic State	Form. Energies (eV)	E _{ads} (eV)	d _{TM-Cl} (Å) (Av)	μ_{Bcell}	μ_{BTM} ,	Q(TM) (e)	ICOHP (TM-3Fe) (eV)	ICOBI (TM-3Fe) (eV)
Sc	FM	-12.08	-2.25	2.53	12.12	-0.70	1.15	-2.55	0.29
Ti	FM	-12.64	-2.80	2.42	11.00	-1.09	1.19	-3.26	0.30
V	FM	-11.84	-2.01	2.32	10.00	-2.24	0.78	-3.26	0.36
Cr	FM	-10.67	-0.84	2.32	9.00	-3.55	0.61	-1.53	0.15
Mn	FM	-10.10	-0.26	2.55	19.00	3.87	0.40	-1.43	0.09
Fe	FM	-11.70	-1.86	2.36	18.00	2.98	0.21	-1.53	0.07
Co	FM	-12.00	-2.16	2.32	17.00	2.04	-0.04	-2.18	0.10
Ni	FM	-11.51	-1.67	2.32	15.55	1.02	-0.04	-1.68	0.10

First, formation energies have been calculated to provide a qualitative interpretation of their experimental synthesizability based on FM and AFM-based ground states. According to Table 3, the formation energies of all structures in magnetic orders that give the lowest energy show that all TM-embedded might be synthesized experimentally. The values related to the distances, ICOHP and ICOBI, are averaged over the number of the neighbors. $\mu_B(TM)$, $\mu_B(Fe)$ (Avg) quantities are given for geometries of the most stable magnetic order. For all layers, FM state has been found as the magnetic ground state based on the geometric optimizations. Transition metals refers to the transition metal embedded FeCl₂ layers. Formation Energies stand for the formation energies. While E_{ads} correspond to the adsorption energies, ΔE_{total} refers to the total energy differences corresponding magnetic structures. Among the reported quantities in Table 3, the adsorption energy is the crucial quantity for the chemical stabilization of embedded transition metals. The largest adsorption energies except Mn are within the chemisorption range, which is generally taken as above 0.6 eV [39]. Therefore, the Mn embedded FeCl₂ layer is not appropriate because of low adsorption energy, which is closer to the lower boundary of the Van der Waals limit. It is important to note that TM-FeCl₂ layers have 4 Fe, 1 TM, and 7 Cl atoms. The total magnetization of all cells is mainly shared by Fe and TM atoms, depending on their magnetic orders. It is found that all of the Fe atoms in the layer have nearly 3 μ B magnetization, which shows they are simultaneously aligned in the same direction. On the contrary, embedded TM atoms have highly varying

magnetization values from -3.55 to 3.87 μ B, which states the usefulness of this strategy in tuning magnetic properties. Considering the bare layers such as TMCl₂ (TM: transition metal), magnetization range is wide in our results [8]. Based on the Bader charges, embedded transition metals donate more electrons to the surrounding Fe atoms from Sc to Ni. This trend nearly follows the Pauling Scale of Electronegativity [40].

Investigating the effect of transition metal embedding on chemical bonding is also very important for practical applications. When looking at the change of the ICOHP parameter between TM and its neighborhoods, it is seen that there is a rough relationship between it and the adsorption energy. For example, the ICOHP value for Fe and Mn atoms is -1.43 eV and -1.53 eV, respectively. When compared with the ICOBI quantity values of 0.09 and 0.07 for the same bonds, it is concluded that the ionic character of the bonds these atoms make with the surrounding Fe atoms is dominant. ICOHP quantities for other metals also comply with ICOBI quantities as expected. This article's primary purpose is to observe electronic behavior by embedding transition metal into Cl defects on the FeCl₂ layer. To reach this aim, spin-dependent PDOS and Band structure curves are crucial to understand. The most critical point in spintronic applications is that regardless of the changes in the structure, conductivity is provided through only a single spin channel.

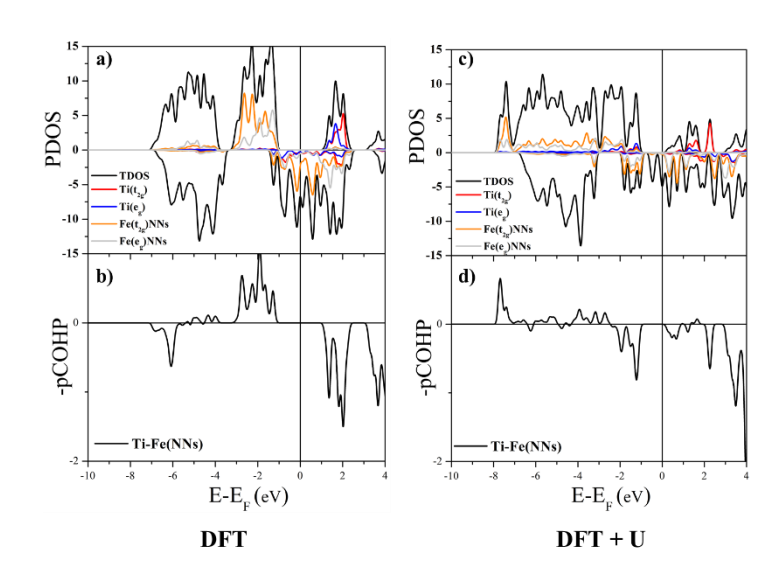


Fig. 4. Projected Density of States and Crystal Orbital Hamiltonian Population curves for (a) Ti-FeCl₂ without U parameter and (b) Ti-FeCl₂ without U parameter. Black, red, blue, orange and green curves correspond to the Total DOS, Ti e_g, Ti t_{2g} orbitals, t_{2g} and eg orbitals of the nearest neighbor Fe to Ti, respectively.

The strong influence of electron correlation on the electronic and magnetic behavior of 2D transition metal (TM) halides arises mainly from the presence of narrow t_{2g} or e_g states near the Fermi level. This complex interplay means that standard density functional theory (DFT) methods, such as LSDA or GGA, often fail to accurately predict their physical properties. As a result, advanced theoretical frameworks like DFT+U are indispensable for a proper description [41]. Hubbard parameters have been taken from the Reference [42]. Because of this reason, the efficient determination of the electronic structures of the TM-FeCl₂ layers have been investigated through the inclusion of the Hubbard U parameters. It is very well known that the crystal field of the neighboring Fe atoms to the embedded transition metal atom undergoes a crystal field splitting [43]. The half-metallicity of the Ti based layer originated from the 3 Fe atoms neighboring the embedded atom. According to Figure 4a, triply degenerate t_{2g} states (d_{xy} , d_{yz} , d_{xz}) and

the doubly degenerate, e.g., states (d_{x2-y2} , d_{z2}) of neighboring Fe atoms are nearly responsible for all electronic states around the Fermi level where there is a minute contribution from Ti atoms. In Fig. 4a, the 3d orbitals of the Ti atom embedded in Cl position show clear interactions with its surrounding Fe atoms at around -1 and -2 eV in spin-up channels. In this regime, the interactions have bonding nature according to the Fig. 4b. It is quite apparent that the conductive behavior of the structure is wholly driven through a spin down channel, which is a half-metallic behavior prerequisite for spintronic applications. Simultaneously, there is a noticeable gap at the spin-up channel. Cl atoms contribute to filling electronic states from -4 eV to the deeper states because TM and Fe contributions are minute. After the inclusion of the Hubbard parameters, the half-metallicity is preserved. The electron conductance is provided through spin-down channel in Fig. 4c, while there is a clear gap at the spin-up channel. According to the pCOHP plots in Fig. 4d, between -1 and -2 eV, the interactions are mainly antibonding. To better understanding the half-metallicity, the picture can be more clear from the band gap plots.

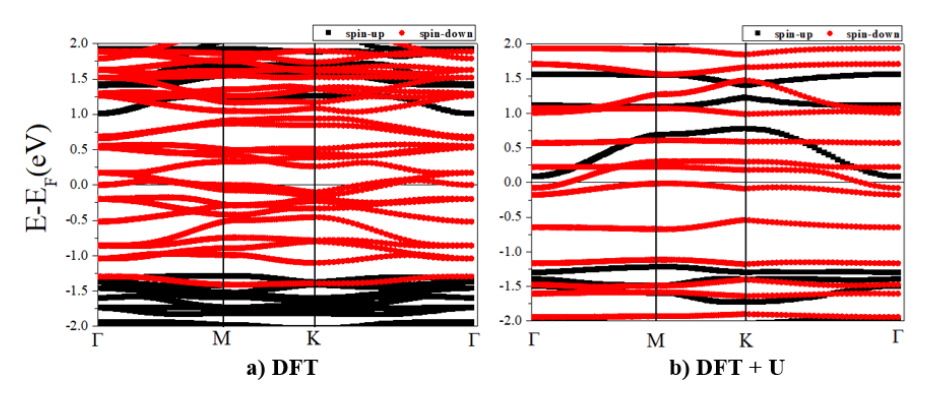


Fig. 5. The calculated band structure plots for the Ti-FeCl₂ layer (a) with DFT and (b) DFT+U. Black and red curves correspond to the bands in spin-up and down channels, respectively.

In Figure 5, spin-polarized electronic band structure figures over the high symmetry points in the Brillouin zones of Ti-FeCl₂ can be seen. In Fig. 5a, where the Hubbard parameters are not included, the conductivity is provided over the spin-down channel which is coherent with the PDOS figures in Fig. 4. Here, the electronic band gap is around 2.5 eV. In Fig. 4b, Ti-FeCl₂ still preserves the half-metallicity although the electronic structure has been dramatically influenced by the U correction. Especially the inclusion of the U parameter into the calculations considerably increases the plausibility of the calculations. The electronic band structure plots for the other layers can be seen between Figs. S2 and S7. From these plots for the other layers, the electronic behavior change is completely between metallicity and semiconductivity.

Conclusions

This article investigated the effect of embedding various transition metals on Cl defects in FeCl₂ material. First, transition metal embedding has been shown to cause a wide range of magnetization values. At this stage, it was determined that Ti-FeCl₂ layers showed half-metallic behavior. The same electronic behavior was observed after the inclusion of the Hubbard U parameter where the Band structure and PDOS plots support each other. Our computations have clarified that the other transition metal embeddings do not provide half-metallicity and electronic behavior swings between metallicity and semiconductivity. Finally, it is suggested that the transition metal embedding strategy in FeCl₂ layers has serious potential for spintronic applications due to the properties as mentioned above.

Acknowledgment

The numerical calculations reported in this paper were completely performed at TUBITAK ULAKBIM, High

Performance and Grid Computing Center (TRUBA resources).

References

- [1] L. Shi and X. Luo, "A first-principles investigation of spintronics of nitrophosphorene doped with 3d transition metals," J. Appl. Phys., vol. 125, no. 23, 2019, doi: 10.1063/1.5089903.
- [2] M. N. Baibich, et al., "Giant magnetoresistance of (001) Fe/(001) Cr magnetic superlattices," Phys. Rev. Lett., vol. 61, no. 21, p. 2472, 1988, doi: 10.1103/PhysRevLett.61.2472.
- [3] I. Khan Muhammad, K. Swera, and M. Abdul, "Computational study of 4d transition metals doped bismuthene for spintronics," Physica E Low-Dimens. Syst. Nanostruct., vol. 126, p. 114464, 2021, doi: 10.1016/j.physe.2020.114464.
- [4] D. Gao, et al., "Defect-related ferromagnetism in ultrathin metal-free gC₃N₄ nanosheets," Nanoscale, vol. 6, no. 5, pp. 2577–2581, 2014, doi: 10.1039/c3nr04743a.
- [5] M. Luo, H. Yin, and Y. Shen, "Magnetic and electronic properties of BN nanosheets with different nonmagnetic metal dopants: A first-principles study," J. Supercond. Nov. Magn., vol. 31, pp. 2211–2216, 2018, doi: 10.1007/s10948-018-4589-8.
- [6] E.-J. Kan, et al., "Half-metallicity in hybrid BCN nanoribbons," J. Chem. Phys., vol. 129, no. 8, 2008, doi: 10.1063/1.2971187.
- [7] K. Li, et al., "First-principles study on ferromagnetism in C-doped AlN," Phys. Lett. A, vol. 374, no. 35, pp. 3671–3675, 2010, doi: 10.1016/j.physleta.2010.07.011.
- [8] A. S. Botana and M. R. Norman, "Electronic structure and magnetism of transition metal dihalides: bulk to monolayer," Phys. Rev. Mater., vol. 3, no. 4, p. 044001, 2019, doi: 10.1103/PhysRevMaterials.3.044001.
- [9] M. Ashton, et al., "Two-dimensional intrinsic half-metals with large spin gaps," Nano Lett., vol. 17, no. 9, pp. 5251–5257, 2017, doi: 10.1021/acs.nanolett.7b01367.
- [10] M. A. McGuire, "Crystal and magnetic structures in layered, transition metal dihalides and trihalides," Crystals, vol. 7, no. 5, p. 121, 2017, doi: 10.3390/cryst7050121.
- [11] X. Zhou, et al., "Atomically thin 1T-FeCl₂ grown by molecular-beam epitaxy," J. Phys. Chem. C, vol. 124, no. 17, pp. 9416–9423, 2020, doi: 10.1021/acs.jpcc.0c03050.
- [12] E. Torun, et al., "Stable half-metallic monolayers of FeCl₂," Appl. Phys. Lett., vol. 106, no. 19, 2015, doi: 10.1063/1.4921096.
- [13] C. Sun and X. Luo, "Tuning the magnetic and electronic properties of monolayer VI₃ by 3d transition metal doping: A first-principles study," Appl. Surf. Sci., vol. 571, p. 151208, 2022, doi: 10.1016/j.apsusc.2021.151208.
- [14] P. Giannozzi, et al., "Advanced capabilities for materials modelling with Quantum ESPRESSO," J. Phys. Condens. Matter, vol. 29, no. 46, p. 465901, 2017, doi: 10.1088/1361-648X/aa8f79.
- [15] P. Giannozzi, et al., "QUANTUM ESPRESSO: a modular and open-source software project for quantum simulations of materials," J. Phys. Condens, Matter, vol. 21, no. 39, p. 395502, 2009, doi: 10.1088/0953-8984/21/39/395502.
- [16] X. Liao, et al., "Density functional theory for electrocatalysis," Energy Environ. Mater., vol. 5, no. 1, pp. 157-185, 2022, doi: 10.1002/eem2.12204.
- [17] P. E. Blöchl, "Projector augmented-wave method," Phys. Rev. B, vol. 50, no. 24, p. 17953, 1994, doi: 10.1103/PhysRevB.50.17953.
- [18] G. Kresse and D. Joubert, "From ultrasoft pseudopotentials to the projector augmented-wave method," Phys. Rev. B, vol. 59, no. 3, p. 1758, 1999, doi: 10.1103/PhysRevB.59.1758.
- [19] J. P. Perdew, K. Burke, and M. Ernzerhof, "Generalized gradient approximation made simple," Phys. Rev. Lett., vol. 77, no. 18, p. 3865, 1996, doi: 10.1103/PhysRevLett.77.3865.
- [20] H. J. Monkhorst and J. D. Pack, "Special points for Brillouin-zone integrations," Phys. Rev. B, vol. 13, no. 12, p. 5188, 1976, doi: 10.1103/PhysRevB.13.5188.
- [21] G. Henkelman, A. Arnaldsson, and H. Jónsson, "A fast and robust algorithm for Bader decomposition of charge density," Comput. Mater. Sci., vol. 36, no. 3, pp. 354–360, 2006, doi: 10.1016/j.commatsci.2005.04.010.
- [22] E. Sanville, et al., "Improved grid based algorithm for Bader charge allocation," J. Comput. Chem., vol. 28, no. 5, pp. 899 908, 2007, doi: 10.1002/jcc.20575.
- [23] W. Tang, E. Sanville, and G. Henkelman, "A grid-based Bader analysis algorithm without lattice bias," J. Phys. Condens. Matter, vol. 21, no. 8, p. 084204, 2009, doi: 10.1088/0953-8984/21/8/084204.
- [24] V. L. Deringer, A. L. Tchougréeff, and R. Dronskowski, "Crystal orbital Hamilton population (COHP) analysis as projected from plane-wave basis sets," J. Phys. Chem. A, vol. 115, no. 21, pp. 5461–5466, 2011, doi: 10.1021/jp202489s.
- [25] R. Dronskowski and P. E. Bloechl, "Crystal orbital Hamilton populations (COHP): energy-resolved visualization of chemical bonding in solids based on density-functional calculations," J. Phys. Chem., vol. 97, no. 33, pp. 8617–8624, 1993, doi: 10.1021/j100135a014.
- [26] R. Y. Rohling, et al., "Electronic structure analysis of the Diels-Alder cycloaddition catalyzed by alkali-exchanged faujasites," J. Phys. Chem. C, vol. 122, no. 26, pp. 14733–14743, 2018, doi: 10.1021/acs.jpcc.8b04409.
- [27] R. Y. Rohling, et al., "Correlations between density-based bond orders and orbital-based bond energies for chemical bonding analysis," J. Phys. Chem. C, vol. 123, no. 5, pp. 2843–2854, 2019, doi: 10.1021/acs.jpcc.8b08934.
- [28] R. Van Santen and I. Tranca, "How molecular is the chemisorptive bond?" Phys. Chem. Chem. Phys., vol. 18, no. 31, pp. 20868–20894, 2016, doi: 10.1039/C6CP01394E.
- [29] R. A. van Santen, I. Tranca, and E. J. Hensen, "Theory of surface chemistry and reactivity of reducible oxides," Catal. Today, vol. 244, pp. 63–84, 2015, doi: 10.1016/j.cattod.2014.07.009.
- [30] P. C. Müller, et al., "Crystal orbital bond index: covalent bond orders in solids," J. Phys. Chem. C, vol. 125, no. 14, pp. 7959–7970, 2021, doi: 10.1021/acs.jpcc.1c00718.

- [31] K. B. Wiberg, "Application of the Pople-Santry-Segal CNDO method to the cyclopropylcarbinyl and cyclobutyl cation and to bicyclobutane," Tetrahedron, vol. 24, no. 3, pp. 1083–1096, 1968, doi: 10.1016/0040-4020(68)88057-3.
- [32] I. Mayer, "Charge, bond order and valence in the AB initio SCF theory," Chem. Phys. Lett., vol. 97, no. 3, pp. 270-274, 1983, doi: 10.1016/0009-2614(83)80005-0.
- [33] S. Maintz, et al., "LOBSTER: A tool to extract chemical bonding from plane wave based DFT," J. Comput. Chem., 2016, doi: 10.1002/jcc.24300.
- [34] S. J. Clark, et al., "First principles methods using CASTEP," Z. Kristallogr., vol. 220, no. 5-6, pp. 567-570, 2005, doi: 10.1524/zkri.220.5.567.65075.
- [35] R. K. Ghosh, A. Jose, and G. Kumari, "Intrinsic spin-dynamical properties of two-dimensional half-metallic FeX₂ (X = Cl, Br, I) ferromagnets: Insight from density functional theory calculations," Phys. Rev. B, vol. 103, no. 5, p. 054409, 2021, doi: 10.1103/PhysRevB.103.054409.
- [36] Yang, Y., et al., "An insulating and easy magnetization-plane magnet: The DFT+ U and constrained electron population study of 1 T-FeCl₂," Computational Materials Science, vol. 233, p. 112752, 2024. https://doi.org/10.1016/j.commatsci.2023.112752
- [37] D. V. Yandulov and R. R. Schrock, "Catalytic reduction of dinitrogen to ammonia at a single molybdenum center," Science, vol. 301, no. 5629, pp. 76–78, 2003, doi: 10.1126/science.1085326.
- [38] E. Dražević and E. Skúlason, "Are there any overlooked catalysts for electrochemical NH₃ synthesis—new insights from analysis of thermochemical data," iScience, vol. 23, no. 12, p. 101803, 2020, doi: 10.1016/j.isci.2020.101803.
- [39] V. Orazi, et al., "DFT study of the hydrogen adsorption and storage on Ni₄ cluster embedded in multivacancy graphene," Int. J. Hydrogen Energy, vol. 45, no. 55, pp. 30805–30817, 2020, doi: 10.1016/j.ijhydene.2020.08.106.
- [40] L. Pauling, "The nature of the chemical bond. IV. The energy of single bonds and the relative electronegativity of atoms," J. Am. Chem. Soc., vol. 54, no. 9, pp. 3570–3582, 1932, doi: 10.1021/ja01348a011.
- [41] Wang, H., V. Eyert, and U. Schwingenschlögl, "Electronic structure and magnetic ordering of the semiconducting chromium trihalides CrCl3, CrBr3, and Crl3". Journal of Physics: Condensed Matter, Vol. 23, no. 11, p. 116003. 2011.doi: 10.1088/0953-8984/23/11/116003
- [42] Yekta, Y., et al., "Strength of effective Coulomb interaction in two-dimensional transition-metal halides MX 2 and MX 3 (M= Ti, V, Cr, Mn, Fe, Co, Ni; X= Cl, Br, I)". Physical Review Materials, Vol. 5, no. 3: p. 034001, 2021. doi: https://doi.org/10.1103/PhysRevMaterials.5.034001
- [43] Y. Feng, et al., "Robust half-metallicities and perfect spin transport properties in 2D transition metal dichlorides," J. Mater. Chem. C, vol. 6, no. 15, pp. 4087–4094, 2018, doi: 10.1039/C8TC00443A.